Title

The Lys-Specific Molecular Tweezer, CLR01, Modulates Aggregation of the Mutant p53 DNA Binding Domain and Inhibits Its Toxicity.

Journal

Biochemistry, 54(24)

ISSN

0006-2960

Authors

Herzog, Gal
Shmueli, Merav D
Levy, Limor
et al.

Publication Date

2015-06-01

DOI

10.1021/bi501092p

Peer reviewed

BIOCHEMISTRY
including biophysical chemistry & molecular biology

Article

The Lys-specific molecular tweezer, CLR01, modulates aggregation of mutant p53 DNA binding domain and inhibits its toxicity

Gal Herzog, Merav Daniel Shmueli, Limor Levy, Liat Engel, Ehud Gazit, Frank-Gerrit Klärner, Thomas Schrader, Gal Bitan, and Daniel Segal

Biochemistry, **Just Accepted Manuscript** • Publication Date (Web): 01 Jun 2015

The Lys-specific molecular tweezer, CLR01, modulates aggregation of mutant p53 DNA binding domain and inhibits its toxicity

Gal Herzog[1§], Merav D. Shmueli[1§], Limor Levy[1], Liat Engel[1], Ehud Gazit[1], Frank-Gerrit Klärner[2] Thomas Schrader[2], Gal Bitan[3] and Daniel Segal[1,]*

[1] Department of Molecular Microbiology and Biotechnology, George S. Wise Faculty of Life Sciences, Tel Aviv University, Ramat Aviv, Israel, 69978. [2] Institute of Organic Chemistry, University of Duisburg-Essen, 45117 Essen, Germany. [3] Department of Neurology, David Geffen School of Medicine, Brain Research Institute, and Molecular Biology Institute, University of California at Los Angeles, Los Angeles, CA 90095-7334, USA

Running title:

Molecular tweezer inhibits mutant p53 aggregation and toxicity

§ Both authors contributed equally to this work.

* Corresponding author: Daniel Segal

Department of Molecular Microbiology and Biotechnology

Tel Aviv University, Tel Aviv 69978, Israel

Phone: ++972-3-6409835

Fax: ++972-3-640-9407

e-mail: dsegal@post.tau.ac.il

ABSTRACT: The tumor suppressor p53 plays a unique role as a central hub of numerous cell proliferation and apoptotic pathways and its malfunction due to mutations is a major cause of various malignancies. Therefore, it serves as an attractive target for developing novel anti-cancer therapeutics. Due to its intrinsically unstable DNA-binding domain, p53 unfolds rapidly at physiological temperature. Certain mutants shift the equilibrium towards the unfolded state and yield high-molecular-weight, non-functional, and cytotoxic β-sheet-rich aggregates that share tinctorial and conformational similarities with amyloid deposits found in various protein-misfolding diseases. Here, we examined the effect of a novel protein-assembly modulator, the lysine (Lys)-specific molecular tweezer, CLR01, on different aggregation stages of misfolded mutant p53 *in vitro* and on the cytotoxicity of the resulting p53 aggregates in cell culture. We found that CLR01 induced rapid formation of β-sheet-rich, intermediate-size p53 aggregates, yet inhibited further p53 aggregation and reduced cytotoxicity of the resulting aggregates. Our data suggest that aggregation modulators, such as CLR01, could prevent formation of toxic p53 aggregates.

INTRODUCTION:

p53 is a transcription factor that regulates cell cycle and plays a key role in the prevention of cancer development (*1*). The outstanding role of p53 as a tumor suppressor and its unique location as a hub of numerous cell pathways make it a prime target for developing novel anti-cancer therapeutics.

p53 functions as a homo-tetramer, comprising four polypeptide chains of 393 amino-acid residues each. The structure of p53 consists of two folded domains: the DNA binding domain (DBD) and the oligomerization domain (OD), which are flanked by intrinsically disordered domains – the trans-activation domain (TAD) in the N-terminus, and a regulatory domain at the extreme C-terminus (CTD). The p53DBD is intrinsically unstable and unfolds rapidly at body temperature (*2, 3*).

Folded and unfolded p53 are in equilibrium, but unfolded p53 can denature irreversibly and form small, soluble aggregates, which subsequently assemble irreversibly by classical nucleation-dependent polymerization, displaying typical kinetics characterized by a lag phase, followed by a rapid growth and finally a plateau (Fig. 1) (*3-5*). This process is facilitated by multiple distinct mutations and eventually yields high molecular weight, β-sheet-rich aggregates that are conformationally and tinctorially similar to the amyloid deposits characterizing many protein-misfolding diseases, although their morphology tends to be amorphous rather than fibrillar (*5-7*).

Because the DBD governs the stability of the entire protein and is responsible for its transcriptional transactivation, >90% of the oncogenic mutations in p53 have been found to be located in this domain (*8*). Of all p53-associated cancer mutations, 30–40% perturb the structure of the protein (conformational mutations), resulting in

reduced thermo-stability and leading to increased aggregation rate (*3, 9*). Two such examples are the mutations leading to G245S and R249S substitutions in the p53 DBD, which are two of the six most frequent conformational mutations in human cancers (*9*). These two mutants and other conformational mutants of p53 largely are unfolded under physiological conditions, thus displaying a loss of transcription transactivation capacity (*10*). The G245S and R249S substitutions induce conformational changes in the DBD and destabilize the protein moderately by only 1-2 kcal/mol (*8*).

The G245S and R249S structural variants of p53 result from two of the most frequent mutation in the p53 cognate gene found in cancer patients. These mutations are located in the L3 loop, which binds to the minor groove of DNA-response elements (*11*). The crystal structure of p53DBD-G245S revealed distinct structural changes in the immediate environment of the mutation site. Observed conformational changes in certain surface loops (e.g., the L1 and S7–S8 loops) can be attributed to differences in crystallization conditions and crystal packing for WT p53DBD and p53DBD-G245S. In contrast, the R249S mutation, substantially perturbs the L3 loop, induces high flexibility, and favors alternative conformations with substantially more severe consequences for the overall protein stability and DNA binding (*11*). These structural changes in p53DBD also result in high propensity of G245S and R249S to aggregate (*3*).

Although a large body of structural information is available on the transition of p53 mutants from the folded to the unfolded state, much less is known about the shift from the unfolded to the "small aggregated" state. It is thus reasonable to believe that because p53DBD-G245S and p53DBD-R249S adopt alternative conformation in the unfolded state they also possess different structures at the initiation of aggregation.

In addition to being non-functional, structural p53 mutants also have been reported to impart a dominant-negative effect over the wild-type protein. A recent landmark paper has uncovered a novel mechanism for this dominant-negative effect. Rousseau, Schymkowitz and coworkers found that the structural mutations expose an aggregation-nucleating sequence, which normally is buried in the hydrophobic core of the DBD of p53. As a result, these mutant proteins have an increased propensity to form amyloid-like aggregates (*12*). In addition, these aggregates recruit wild-type p53 into cellular inclusions thereby decreasing the normal p53 availability and accounting for the dominant-negative effect of the mutant. Moreover, structurally destabilized p53 mutants also co-aggregate with the p53 family members p63 and p73, thereby accounting for their loss of function (*12*).

Interestingly, it has been shown recently that pre-formed p53 aggregates enter HeLa cells via macropinocytosis, a non-specific pathway, and induce intracellular aggregation of endogenous p53 (*13*). Although the clinical significance of this observation remains to be elucidated, these data suggest a possible role for p53 aggregation in cancer development that is distinct from direct loss of function of p53 by mutation. Thus, interfering with the aggregation of p53 mutants by small-molecule modulators may prevent the harmful effects of the resulting aggregates and co-aggregation with WT p53, p63, and p73. However, rescuing folding and function of p53 mutants by a specific ligand represents a great challenge because only few of these mutants (e.g., Y220C) possess a cleft or a crevice that can be targeted by a small molecule without interfering with the ability of p53 to bind its DNA response element (*11*). An alternative strategy is to modulate the aggregation itself. Theoretically, if a small molecule could prevent the formation of the amyloid-like aggregates, it might

both prevent the potential toxicity of these aggregates and inhibit the recruitment of wild-type p53, p63 and p73 into the aggregates.

Recently, a novel family of protein-assembly modulators, namely Lysine (Lys)-specific molecular tweezers (MTs), was found to be highly efficient inhibitors of amyloid assembly and toxicity (*14*). These small molecules are horseshoe-shaped, artificial Lys receptors composed of two hydrocarbon arms capable of hydrophobic interactions with the alkyl side chains of Lys residues, and negatively charged head groups that form electrostatic interactions with the NH_3^+ group of Lys (Fig. 2).

Inhibition of aggregation by MTs is selective for amyloidogenic proteins but is not specific to a particular protein (*15*). For example, the MT, CLR01 (Fig. 2a), disrupted *in vitro* the aggregation and toxicity of multiple disease-related proteins, such as amyloid β-protein (Aβ), tau and α-synuclein at equimolar or sub-equimolar concentration ratios (*14*), whereas disruption of tubulin polymerization required ~55-fold excess of CLR01 (*15*) and inhibition of enzymatic activity, e.g., of alcohol dehydrogenase, required ~850-fold excess CLR01 (*16*). In agreement with these observations, *in vivo* CLR01 suppressed α-synuclein aggregation in neurons and rescued the phenotype and survival of zebrafish embryos (*17*), cleared existing Aβ and tau aggregates in the brain of Alzheimer's disease transgenic mice, and decreased transthyretin aggregation in a mouse model of familial amyloidotic polyneuropathy, without any side effects (*17-19*). Moreover, CLR01 was found to have a high safety margin in mice (*15*), supporting its selective action as an inhibitor of abnormal protein aggregation.

Here, we examined the effect of CLR01 on different stages of aggregation of the p53 mutants G245S and R249S *in vitro* and on the harmful effect of their pre-formed aggregates in cultured lung carcinoma cells. We found that CLR01 induced rapid

formation of β-sheet-rich, intermediate-size aggregates by each p53DBD mutant, inhibited formation of later aggregates, and reduced the cytotoxicity of the resulting aggregates.

MATERIALS AND METHODS

The Na^+ salts of CLR01 and CLR03 were prepared and purified analogously to the Li salts, as described previously (*16*).

Cloning: The coding sequence of the gene encoding human p53DBD was amplified using the primers 5'-GGGAATTCGGATCCATGTCATCTTCTGTCCCTTCCCAG-3' and 5'-TCTGACCTCGAGTCAGGTGTTGTTGGACAGTGCTCGC-3'. The G245S-p53DBD mutant or R249S-p53DBD were generated by PCR site-directed mutagenesis using the primer 5'-CTGCATGGGCaGCATGAACC-3' or 5'-CATGAACCGGAGcCCCATC-3', respectively (lower-case letter indicates the substitution made to produce the mutation). The PCR products were digested with *Bam*HI and *Xho*I, purified, and cloned into a modified pET24a+ expression vector. The resulting plasmids encoded fusion proteins comprising an N-terminal 6×His-tag, the lipoyl domain of the dihydrolipoamide acetyltransferase from *Bacillus stearothermophilus*, and a TEV-protease cleavage site followed by p53DBD.

Protein expression and purification: The appropriate vector was transformed into competent E. *coli* BL21 tuner cells (Novagen) for overexpression. Expression cultures were incubated at 37°C with shaking at 220 rpm until OD_{600} reached 0.7-0.8. The medium was supplemented with 0.1 mM $ZnSO_4$ and expression was induced with 0.5 mM Isopropyl β-D-1-thiogalactopyranoside at 18 °C. Cells were harvested 14 hours later by centrifugation. The cell pellet from 3 liters of culture was suspended in 50

mM Tris-HCl, pH 7.2, 200 mM NaCl, 0.8% triton, 10% glycerol, 5 mM imidazole, 10 mM β-mercaptoethanol and X50 tablets of EDTA-free complete protease inhibitor (Roche). Cells were sonicated on ice for a total time of 8 minutes, with 90 seconds in between 30-second pulses. The soluble fraction was loaded onto an Amersham 26/20 column packed with Ni-Sepharose (GE-Healthcare). The His-tagged fusion protein was eluted using a 0–500 mM imidazole gradient over ten column volumes. The pooled fractions from the Ni-Sepharose column were digested with TEV protease overnight and dialyzed against a low-salt buffer containing 50 mM Tris-HCl, pH 7.2, 50 mM NaCl, 10% glycerol and 10 mM β-mercaptoethanol. The dialyzed sample was purified further on a HiPrep Heparin 16/10 FF ion-exchange column (GE-Healthcare). Elution was done using a 0-500 mM NaCl gradient over 10 column volumes. The pooled fractions were concentrated using an Amicon ultra-15 with a 30-kDa cutoff (Millipore) and buffer-exchanged to 25 mM sodium phosphate, pH 7.2, 10% glycerol, 300 mM NaCl and 1 mM *tris* 2-carboxyethyl phosphine (TCEP). To obtain high-purity proteins, a final gel-filtration step was carried out. Gel-filtration column (Superdex 75 HiLoad 16/60, GE Healthcare) was equilibrated with 25 mM sodium phosphate, pH 7.2, 10% glycerol, 300 mM NaCl and 1 mM TCEP. The loading volume of concentrated proteins was 0.5 mL per run. Separation was carried out by running 1.5 column volumes of the buffer and collecting 0.5 mL fractions. Protein samples were flash-frozen and stored in liquid nitrogen for further use. The purified p53 variants were verified by Western blot analysis under denaturing conditions using an anti-p53 monoclonal antibody (PAb 240, Abcam).

Differential scanning fluorimetry (DSF): Experiments were performed using SYPRO Orange (Invitrogen) as the fluorescent probe, which binds quantitatively to the hydrophobic protein patches exposed upon thermal denaturation. Real-time melting

analysis was performed using a Corbett Rotor-Gene 6000 real-time qPCR thermocycler. The excitation (λ_{ex}) and emission (λ_{em}) wavelengths used were 460 nm and 510 nm, respectively. Heating from 28 to 70°C was applied at a constant heating rate of 250°C/h. 10 μM of the protein were briefly mixed with SYPRO orange (10×) in 25 mM sodium phosphate buffer, pH 7.2, 300 mM NaCl, 10% glycerol, 10% DMSO and 1 mM TCEP. The apparent melting temperature (T_m) of the protein was determined from the inflection point of the melting curve.

Static light scattering (SLS): Protein aggregation was monitored by measuring static light scattering at 500 nm as excitation and emission wavelengths (excitation slit width 0.8 nm, emission slit width 2 nm) using a Horiba (Kyoto, Japan) FluoroMax-3 spectrophotometer. Experiments were performed using G245S-p53DBD or R249S-p53DBD at concentration of 3 μM in 25 mM sodium phosphate, pH 7.2, 300 mM NaCl, 5% DMSO and 1 mM TCEP buffer that was pre-equilibrated for 30 min at 37 °C. The samples were stirred constantly. Data were analyzed using Kaleidagraph™ software (Synergy).

Thioflavin-T (ThT) assay: ThT fluorescence was measured at 482 nm upon excitation at 450 nm for detecting β-sheet formation (excitation slit width 3 nm, emission slit width 4 nm), using a Horiba FluoroMax-3 spectrofluorometer. Time-resolved fluorescence was recorded immediately after adding 3 μM of G245S-p53DBD or R249S-p53DBD protein to pre-equilibrated buffer (25 mM sodium phosphate, pH 7.2, 300 mM NaCl, 5% DMSO, 1 mM TCEP and 10 μM ThT.

8-Anilino-1-naphthalene Sulfonic Acid (ANS) binding assay: ANS fluorescence was measured at 465 nm upon excitation at 350 nm for monitoring exposed hydrophobic regions in proteins, using a Horiba Jobin Yvon FL3-11 spectrofluorometer. Time-resolved fluorescence was recorded immediately after adding 5 μM of G245S-

p53DBD or R249S-p53DBD proteins to pre-equilibrated buffer (25 mM sodium phosphate, pH 7.2, 300 mM NaCl, 5% DMSO, 1 mM TCEP, different concentrations of the tested compounds, and 5 μM ANS.

Circular dichroism (CD) Measurements: CD spectra at far UV (200-250 nm) was recorded with a Chirascan™ CD Spectrometer (Applied Photophysics) equipped with a temperaturecontrolled cell using a cell of pathlength 0.5 cm. Bandwidth was 1 nm, and averaging time was 30 sec for each measurement. Protein concentration was 5 μM in a buffer containing 25 mM sodium phosphate, pH 7.2, 100 mM NaCl, 1 mM TCEP and different concentrations of the tested compounds. The measurements were conducted at 37 °C after 20 min incubation. The percentage of secondary structure calculated using the CDNN software (*20*).

Dot blot: 50 μl spots containing 5 μM protein and different concentrations of the tested compounds, after 20 min incubation at 37 °C, were applied, interspaced with spots containing only buffer, to a nitrocellulose membrane using Minifold I Dot-Blot 96 Well Plate System (Whatman). The membrane was blocked for 1h in blocking solution (5% nonfat milk powder in Tris-buffered saline (TBS)), and then incubated in 1:1000 dilution of the OC antibody (a generous gift from Dr. Rakez Kayed, University of Texas Medical Branch, Galveston, TX) in blocking solution. The membrane was then washed three times for 15min each in TTBS (0.1% Tween-20 in TBS), incubated for 40 min in the anti-rabbit secondary antibody and washed three times for 10 min in TTBS. The membrane was developed using EZ-ECL (Biological Industries, Israel), according to the manufacturer's instructions, and exposed to Fuji Medical X-Ray Film for up to 5 min. Films were developed using Kodak X-OMAT 2000.

Turbidity assay: The aggregation of G245S-p53DBD or R249S-p53DBD protein was monitored by absorbance reading at λ = 340 nm. Samples were incubated in 96-well plates in triplicates, each consisting of 5 μM of the protein dissolved in 25 mM sodium phosphate, pH 7.2, 300 mM NaCl, 5% DMSO, 1 mM TCEP and different concentrations of the tested compound. A similar set of samples including only the tested compound was measured in parallel for background turbidity subtraction. Plates were sealed and transferred immediately to an EL808 plate reader (BioTek). Aggregation was monitored for 2 hours in 3-minute intervals.

Transmission Electron Microscopy: G245S-p53DBD or R249S-p53DBD (5 μM) were incubated at 37 °C in 25 mM sodium phosphate, pH 7.2, 300 mM NaCl, 5% DMSO, 1 mM TCEP and different concentrations of the tested compounds. 5 μL aliquots were taken after 45 min, adsorbed onto freshly glow-discharged carbon-film, 400-mesh copper grids, rinsed with deionized water, and stained with 1% uranyl acetate. Images were taken using a Phillips 208S transmission electron microscope at 80 kV.

Cell viability assay: G245S-p53DBD or R249S-p53DBD aggregates (5 μM) were obtained by overnight incubation at 37 °C in the absence or presence of either CLR01 or CLR03 at different concentrations. The pre-formed aggregates were added to human H1299 non-small cell lung carcinoma cells and incubated for 24 hours. Cell viability was measured using the (2,3-bis-(2-methoxy-4-nitro-5-sulfophenyl)-2H-tetrazolium-5-carboxanilide) (XTT) reduction assay according to the manufacturer´s recommendations (Biological Industries Ltd, Israel) with 3 wells per condition. As a negative control, CLR01 or CLR03 at different concentrations without G245S-p53DBD or R249S-p53DBD aggregates were added to cells. For a positive control, 0.1% Triton-X100 was used for induced cell lethality.

RESULTS

CLR01 does not affect the thermo-stability of the structural mutant G245S-p53DBD

Inactivation of p53 by denaturation involves the initial unfolding of the core domain, which occurs naturally but is reversible (Fig. 1). It was shown previously that CLR01 had no stabilizing effect on other amyloidogenic proteins such as transthyretin (TTR) (*19*). Similarly, MTs would not be expected to stabilize the native conformation of p53, however, they could do that serendipitously, complicating data interpretation. Therefore, to rule out this possibility, CLR01 and the negative control derivative, CLR03, (Fig. 2b), were tested *in vitro* for potential stabilizing effects towards the oncogenic p53DBD structural mutant G245S.

We used differential scanning fluorimetry to measure whether increased concentrations of CLR01 affected the thermodynamic stability of G245S-p53DBD. Concentrations below 100 μM of CLR01 did not affect the apparent T_m of G245S-p53DBD (Fig. 3). At higher concentrations, CLR01 destabilized the protein. Therefore, we set 100 μM as the maximum concentration for further analysis. CLR03, which served as a negative control, had no effect on the apparent T_m of the protein, as expected.

CLR01 induces rapid formation of intermediate, β-sheet-rich, mutant p53DBD aggregates.

Aggregation of p53DBD is accompanied by a conformational transition into amyloid-like structures characterized by a high β-sheet content that can be measured using ThT binding (*6*). Alterations of the pH may influence aggregation rates dramatically (*6*). Therefore, we measured the effect of increased concentrations of CLR01 or CLR03

on the pH of the solution and found that CLR01 or CLR03 caused little change in the pH up to the highest concentration examined – 100 μM (Fig. S1).

ThT binding is independent of the size of protein aggregates. Therefore, it is useful for monitoring the early stages of p53DBD aggregation (*5*). Using this method, we found that at a protein:CLR molar ratio of 1:5, respectively, CLR01 rapidly enhanced ThT binding by G245S-p53DBD (Fig. 4), suggesting induction of formation of a β-sheet-rich structure. This effect was similar to that reported previously by Sinha et al. for insulin, β_2-microglobulin, and TTR (*14*), though the experiments in that study had substantially lower time resolution than measured here. Therefore they observed a high ThT fluorescence signal already at the earliest time point measured, whereas we monitored the development of the signal during the first ~30 seconds.

Next, we used circular dichroism (CD) spectroscopy to evaluate the secondary structure of the G245S-p53DBD mutant in the presence of increased molar ratios of CLR01. In the absence of CLR01, G245S-p53DBD displayed typical α-helix-rich CD spectra characterized by minima at ~207 and 220 nm, in which the 207 nm minimum was slightly lower than the one at 220 nm (Fig. 5) as previously reported (*21*). In the presence of CLR01, a shift was evident towards a β-sheet-rich structure, characterized by a single minimum at 216 nm (Fig. 5). In contrast, CLR03 had no effect on the conformation of G245S-p53DBD, as expected. These CD results corroborated the ThT data.

We also used dot blots with antibody OC, which specifically recognizes β-sheet-rich amyloid fibrils (*22*), to examine the effect of CLR01 on aggregation of G245S-p53DBD. We found that increased concentrations of CLR01 (up to 5-fold excess) resulted in higher OC binding, suggesting enrichment of β-sheet-rich structures (Fig. 6). To examine whether this effect was specific for the G245S mutant, we studied

similarly an additional structural p53DBD mutant, R249S (*23*). In the presence of CLR01, R249S-p53DBD also displayed enrichment of β-sheet-rich structures. This result indicated that the effect of CLR01 was not unique to G245S-p53DBD. Surprisingly, in the presence of CLR03, R249S-p53DBD, but not G245S-p53DBD also showed a moderate increase in OC binding, demonstrating a different behavior of the two p53DBD variants (Fig. 6).

We examined further the effect of CLR01 on aggregation of G245S-p53DBD using static light scattering, which is most effective for monitoring intermediate-size assemblies. The experiments showed dose-dependent acceleration of the aggregation reaction, resulting both from shortening of the lag phase, and from an increase in aggregate-growth rate (Fig. 7). At the highest molar ratio examined, 1:10 protein:CLR01, respectively, the reaction plateaued at ~500 seconds. Together, the ThT fluorescence, CD spectra, OC binding and static light scattering data suggest that upon binding of CLR01 to G245S-p53DBD, the protein rapidly forms β-sheet-rich, intermediate-size aggregates. In contrast, binding of CLR03 to G245S-p53DBD had no effect on the protein aggregation, as expected.

To further investigate the conformational changes of G245S-p53DBD or R249S-p53DBD induced by CLR01, we measured the change in fluorescence upon binding of ANS, a common probe for exposed hydrophobic regions in proteins (*24*). When ANS is free in solution, its fluorescence emission is negligible, but once it binds to hydrophobic patches, its fluorescence emission increases (*25*). Consequently, ANS has been used widely for characterizing intermediate states of proteins such as the molten globule state (*26*). We found that CLR01 binding to the p53DBD mutants G245S or R249S dramatically reduced ANS emission by ~6- and ~4-fold, respectively, compared to the untreated proteins. This low ANS emission was evident

both by the rate and by the amplitude of ANS binding. This suggests that CLR01 reduces exposure of hydrophobic residues in the protein already at the early stages of the folding-unfolding equilibrium of the p53DBD mutants, and further when aggregation is initiated. Interestingly, CLR03 had no effect on G245S-p53DBD, as expected, but slightly reduced ANS emission of R249S-p53DBD (Fig. 8), in agreement with the differences observed between the two p53DBD mutants in OC binding.

Collectively, our results suggest that CLR01 induces formation of β-sheet-rich structures in the p53DBD mutants studied and simultaneously inhibits the exposure of hydrophobic pockets in these proteins, presumably by inducing sequestration of hydrophobic patches through intermolecular association and formation of intermediate-size aggregates.

CLR01 inhibits the late stages of mutant p53DBD aggregation

To monitor the effect of molecular tweezers on the formation rate of the late stages of G245S-p53DBD or R249S-p53DBD aggregation and on the morphology of the resulting aggregates, proteins were incubated in the absence or presence of increasing concentrations of MTs and the reaction was monitored using turbidity and transmission electron microscopy (TEM). R249S-p53DBD exhibited faster and higher degree of aggregation compared to G245S-p53DBD, correlating with the kinetics observed in the ANS binding assay (Fig. 8 and reference (*3*)).

Consistent with the results obtained in the ThT, CD, OC-antibody binding and static light scattering experiments described above, the initial turbidity of the solution in the presence of 1:1 molar ratio of CLR01 was higher than the turbidity of G245S-p53DBD or the same as R249S-p53DBD alone. However, whereas in the solution containing G245S-p53DBD on its own, a lag phase of ~25 minutes was observed

before the turbidity increased, in the presence of CLR01 the turbidity decreased in the first 15 minutes and then began to increase (Fig 9a). Interestingly, at a molar ratio of 1:1 protein:CLR01, respectively, the amplitude of the turbidity was higher than that of G245S-p53DBD alone, whereas at a molar ratio of 1:2 protein:CLR01, respectively, the turbidity amplitude was similar to that of G245S-p53DBD alone.

Increasing the concentration of CLR01 to a molar ratio of 1:5 protein:CLR01, respectively, resulted in decreased turbidity and at a molar ratio of 1:8 protein:CLR01, respectively, no change of turbidity was observed throughout the experiment, suggesting that at this concentration, aggregation was inhibited completely (Fig. 9). Similar results were observed with R249S-p53DBD, which is less folded than G245S (9). CLR01 inhibited the aggregation of R249S-p53DBD in a dose-dependent manner starting at a 1:1 ratio (Fig. 9), though in this case, CLR01 inhibited the growth-rate of R249S-p53DBD, but not its nucleation rate. CLR03 did not affect the aggregation of the p53DBD mutants measured by turbidity, as expected (Fig.9). These results recapitulate the previously reported inhibitory effect of CLR01 on the aggregation of other amyloidogenic proteins (*14, 27*).

TEM analysis indicated that in the presence of CLR01 the p53DBD mutant aggregates were smaller and more dispersed (Fig. 10). Higher magnification images revealed occasional small, curvilinear fibrils (Fig. 10C). Interestingly, at 1:10 protein:CLR01 molar ratio, the aggregates were less dispersed. CLR03 had no effect on G245S-p53DBD aggregates but did reduce R249S-p53DBD aggregates. Both MTs had little effect on the morphology of the aggregates (Fig. 10).

Taken together, the results described above indicate that CLR01 enhances self-assembly of the p53DBD mutants examined into β-sheet-rich structures. Apparently, however, these structures are “off pathway” for formation of typical later-stage

p53DBD mutant aggregates because the kinetics of formation of the later-stage aggregates and the final amount of these aggregates are reduced in the presence of CLR01 in a dose-dependent manner. The modulatory activity of CLR01 requires the hydrophobic side arms of the molecular tweezer, because the negative control CLR03 shows little or no effect on the aggregation of the p53DBD mutants.

CLR01 reduces the toxicity of p53DBD aggregates.

The next important question was whether the assemblies stabilized by CLR01 were cytotoxic. Introduction of *in vitro* pre-formed aggregates of p53DBD mutants to cells has been reported to reduce cell viability (*6*), similarly to other amyloidogenic proteins (*14, 28*). We examined next whether the MTs affect this cytotoxicity in H1299 lung carcinoma cells. CLR01 was reported to be non-toxic in differentiated PC-12 cells up to 200 μM and to induce mild toxicity at 400 μM (*14*). However, toxicity can vary depending on the cell line used. Therefore, we tested the effect of CLR01 and CLR03 on H1299 cells. We found that in agreement with the results reported in PC-12 cells and primary neurons (*29*), CLR01 at 10-100 μM, and CLR03 at 100 μM were not cytotoxic (Fig. S2).

To test the effect of the MTs on cytotoxicity induced by mutant p53DBD we incubated pre-formed G245S-p53DBD or R249S-p53DBD aggregates with CLR01 at molar ratios from 1:2-1:10 or CLR03 at 1:10, respectively, and applied the mixtures to H1299 cells. CLR01 protected the cells significantly from the harmful effect of G245S-p53DBD or R249S-p53DBD aggregates (Fig. 11). The protective effect displayed hormetic behavior as at a 1:10 molar ratio, lower, non-significant protection was observed. Thus, the maximal protection was observed at 1:5 and 1:2 molar ratio for G245S-p53DBD and R249S-p53DBD, respectively. This was not due to toxicity of CLR01 itself, as shown in Figure S2, and at this point the basis for this behavior is

not clear. Interestingly, CLR03 had a significant, dose-independent rescue effect on the viability of R249S-p53DBD-treated cells. This may reflect its moderate effect on R249S-p53DBD observed in the OC, ANS binding, and TEM.

DISCUSSION

Aggregation of p53 conformational mutants has gained recent interest because it accounts for both their dominant-negative and gain of toxic function effects. Our findings that aggregation of p53 mutants converts their native conformation into a β-sheet rich, amyloid-like structure are in line with recent data reported by other groups which used Congo-red staining and ThT fluorescence for monitoring β-sheet structures, as well as recognition by antibody A11, which binds specifically to oligomers of amyloidogenic proteins (*5, 6*). Thus, cancers resulting from misfolded p53 may belong to the broad spectrum of diseases called amyloidoses, including Alzheimer's disease, Parkinson's disease, prion diseases and amyotrophic lateral sclerosis, which are caused by abnormal misfolding and aggregation of amyloidogenic proteins (*30-32*). This novel view of p53 aggregation suggests that therapeutics based on modulating aggregation of amyloidogenic proteins also may be effective against p53 aggregation and the cytotoxicity of the resulting aggregates.

The proposed mechanism of action of CLR01 is binding selectively to exposed Lys residues (and to a lower extent to Arg residues), thereby disrupting hydrophobic and electrostatic interactions that mediate oligomerization and aggregation of amyloidogenic proteins and preventing their toxicity (*33*). The selectivity of the compound is based on the fact that the forces controlling the abnormal aggregation process are relatively weak, hence the oligomers are unstable and are in a dynamic

quasi-equilibrium. The binding of CLR01 is highly labile (*34*) and of moderate (micromolar) affinity, and therefore does not interfere with the structure or function of normal proteins, whose three-dimensional structure has been optimized by millions of years of evolution.

The recent suggestion that p53 aggregates into amyloid-like structures (*5, 12, 30-32, 35*) prompted us to examine if CLR01 could inhibit aggregation and toxicity of "conformational" p53 mutants. In the 393-residue sequence of the native p53 monomer there are 20 Lys (5.1%) and 26 Arg (6.6%) residues, whereas in the 179-residue DBD, the Arg content is higher, 8.9% and the Lys content is 2.2%. These numbers are on par with amyloidogenic proteins studied previously (*14*) and suggested that CLR01 might be able to inhibit the aggregation of mutant p53 and the toxicity of the aggregates.

Of the amyloidogenic proteins for which CLR01's inhibitory activity was studied previously (*14, 27, 36, 37*), Aβ40, Aβ42, tau, α-synuclein and islet amyloid polypeptide are intrinsically disordered, insulin, β_2-microglobulin, and TTR are natively structured, and calcitonin is a relatively short peptide that is partially structured in aqueous solution. Analysis of the behavior of the mixture of each of these proteins with CLR01 in ThT fluorescence or turbidity experiments (*14*) revealed a pattern. For intrinsically disordered proteins, initial ThT binding was minimal and the fluorescence in the beginning of the aggregation reaction was close to background values. In contrast, for the natively structured proteins, the initial ThT fluorescence/turbidity signal was substantially higher in the presence of CLR01 than in its absence, suggesting that binding of CLR01 rapidly induced formation of aggregates in which the β-sheet content was increased relative to the CLR01-unbound state. In the case of calcitonin, the increase in the initial ThT fluorescence was small

relative to the structured proteins, as would be expected for a partially structured peptide (*14*).

Because similarly to insulin, β_2-microglobulin, and TTR, p53 has a well-defined stable structure, we expected that upon interaction with G245S-p53DBD or R249S-p53DBD, CLR01 would induce formation of β-sheet-rich aggregates. This was indeed what we found. Turbidity measurements showed that at the initial time points, larger aggregates were present in samples of G245S-p53DBD or R249S-p53DBD in the presence of CLR01 than in its absence (Fig. 9). Therefore, we conducted ThT fluorescence, CD spectra, OC binding, ANS fluorescence and static light scattering experiments with higher time-resolution than the experiments conducted previously with other proteins or the turbidity measurements performed here. Using the higher time-resolution, we observed the rapid formation of β-sheet-rich, intermediate-size, G245S-p53DBD:CLR01 complexes within ~1 min of mixing the protein and the molecular tweezer (Figs. 4, 7). Examination by TEM, and static light scattering experiments, showed that the size and morphology of the initial G245S-p53DBD and R249S-p53DBD aggregates formed in the absence or presence of CLR01 were similar (Fig. 10), suggesting that the differences between the two types of aggregates were subtle and deciphering these differences would require higher spatial-resolution methods.

Similarly to other amyloidogenic proteins, p53 aggregation is thought to occur via nucleation-dependent polymerization (*5*), characterized by a slow nucleation step followed by fast growth of aggregates (*38*). Our observations support this model. We found that the initial stage of aggregation of the mutant p53 examined occurs at a slow rate followed by a rapid phase of aggregation evidenced by a steep slope (indicated as L and F, respectively in Fig. 9). The final stage is a decrease in the rate

of aggregation and ultimately a plateau, as the system reaches equilibrium (P in Fig. 9). During the final slow step, formation of larger aggregates by association of smaller ones is thought to be a secondary mechanism, though it is difficult to distinguish kinetically from the growth of individual aggregates by currently available techniques. Our data suggest that binding of CLR01 greatly accelerated a nucleation-like phase of G245S-p53DBD or R249S-p53DBD, but the protein:CLR01 assemblies/nuclei had a distinct, off-pathway structure from that of these proteins alone. The hetero-assemblies of G245S-p53DBD or R249S-p53DBD with CLR01 did not promote further growth or propagation of the β-sheet structure. Importantly, these hetero-assemblies had reduced toxicity relative to those formed by G245S-p53DBD or R249S-p53DBD alone.

Cellular effects of p53 aggregation in cancer are associated with cell survival and proliferation rather than with cell death, in contrast to neurodegeneration. However, our cell viability results support recent findings showing that *in vitro* pre-formed aggregates of mutant p53 are cytotoxic (*13*) and suggest that CLR01 can protect cells from this cytotoxicity, in agreement with its effect on other amyloidogenic proteins.

Interestingly, though CLR03 was used as a negative control and was not expected to affect the aggregation or toxicity of the p53DBD mutants, we found that it moderately increased OC binding and decreased ANS binding, selectively to R249S-p53DBD. In correlation with these data, CLR03 also showed moderate, dose-independent protection of H1299 cells against the toxicity of R249S-p53DBD, suggesting that it might promote formation of non-toxic aggregates by a currently unknown mechanism. In most of the studies reported to date CLR03 was found to behave as a negative control, i.e., did not affect the proteins under study where CLR01 had a clear impact. This was the case also in all the experiments we performed using G245S-

p53DBD. In a recent study, CLR03 was found to induce moderate enhancement of oligomerization of Aβ40 and Aβ42 using ion-mobility spectroscopy–mass-spectrometry (*39*), similar to its effect on G245S-p53DBD. The basis for this activity currently is unknown.

Conformational p53 mutants co-aggregate with wild-type p53 in cells (*12*). If this were also the case *in vivo*, this aggregation would result in even lower availability of the wild-type protein, and a higher propensity for malignant cell proliferation. Ideally, inhibition of the abnormal aggregation of mutant p53 would lead to degradation of the misfolded, mutant protein, and release of the normal, wild-type protein, increasing its availability for DNA transcription regulation. Our data suggest that the use of aggregation modulators, such as CLR01, could lead to selective degradation of misfolded p53, thereby increasing the availability of normal p53. Determining the extent of the protective effect provided by inhibiting the aggregation of mutant p53 will require further investigation.

Description of Supporting Information

Supplementary figures show effect of increased concentrations of molecular tweezers on the pH of the buffer (Fig. S1) and on cell viability (Fig. S2). This material is available free of charge via the Internet at http://pubs.acs.org.

References:

1. Lane, D. P. (1992) Cancer. p53, guardian of the genome, *Nature 358*, 15-16.
2. Bullock, A. N., Henckel, J., DeDecker, B. S., Johnson, C. M., Nikolova, P. V., Proctor, M. R., Lane, D. P., and Fersht, A. R. (1997) Thermodynamic stability of wild-type and mutant p53 core domain, *Proc Natl Acad Sci U S A 94*, 14338-14342.
3. Friedler, A., Veprintsev, D. B., Hansson, L. O., and Fersht, A. R. (2003) Kinetic instability of p53 core domain mutants: implications for rescue by small molecules, *The Journal of biological chemistry 278*, 24108-24112.

4. Bullock, A. N., Henckel, J., and Fersht, A. R. (2000) Quantitative analysis of residual folding and DNA binding in mutant p53 core domain: definition of mutant states for rescue in cancer therapy, *Oncogene 19*, 1245-1256.

5. Wilcken, R., Wang, G., Boeckler, F. M., and Fersht, A. R. (2012) Kinetic mechanism of p53 oncogenic mutant aggregation and its inhibition, *Proc. Natl. Acad. Sci. USA 109*, 13584-13589.

6. Ano Bom, A. P., Rangel, L. P., Costa, D. C., de Oliveira, G. A., Sanches, D., Braga, C. A., Gava, L. M., Ramos, C. H., Cepeda, A. O., Stumbo, A. C., De Moura Gallo, C. V., Cordeiro, Y., and Silva, J. L. (2012) Mutant p53 aggregates into prion-like amyloid oligomers and fibrils: implications for cancer, *J. Biol. Chem. 287*, 28152-28162.

7. Ishimaru, D., Andrade, L. R., Teixeira, L. S., Quesado, P. A., Maiolino, L. M., Lopez, P. M., Cordeiro, Y., Costa, L. T., Heckl, W. M., Weissmuller, G., Foguel, D., and Silva, J. L. (2003) Fibrillar aggregates of the tumor suppressor p53 core domain, *Biochemistry 42*, 9022-9027.

8. Olivier, M., Eeles, R., Hollstein, M., Khan, M. A., Harris, C. C., and Hainaut, P. (2002) The IARC TP53 database: new online mutation analysis and recommendations to users, *Hum Mutat 19*, 607-614.

9. Joerger, A. C., and Fersht, A. R. (2007) Structure-function-rescue: the diverse nature of common p53 cancer mutants, *Oncogene 26*, 2226-2242.

10. Joerger, A. C., and Fersht, A. R. (2008) Structural biology of the tumor suppressor p53, *Annu Rev Biochem 77*, 557-582.

11. Joerger, A. C., Ang, H. C., and Fersht, A. R. (2006) Structural basis for understanding oncogenic p53 mutations and designing rescue drugs, *Proceedings of the National Academy of Sciences of the United States of America 103*, 15056-15061.

12. Xu, J., Reumers, J., Couceiro, J. R., De Smet, F., Gallardo, R., Rudyak, S., Cornelis, A., Rozenski, J., Zwolinska, A., Marine, J. C., Lambrechts, D., Suh, Y. A., Rousseau, F., and Schymkowitz, J. (2011) Gain of function of mutant p53 by coaggregation with multiple tumor suppressors, *Nat. Chem. Biol. 7*, 285-295.

13. Forget, K. J., Tremblay, G., and Roucou, X. (2013) p53 Aggregates penetrate cells and induce the co-aggregation of intracellular p53, *PLoS One 8*, e69242.

14. Sinha, S., Lopes, D. H., Du, Z., Pang, E. S., Shanmugam, A., Lomakin, A., Talbiersky, P., Tennstaedt, A., McDaniel, K., Bakshi, R., Kuo, P. Y., Ehrmann, M., Benedek, G. B., Loo, J. A., Klärner, F. G., Schrader, T., Wang, C., and Bitan, G. (2011) Lysine-specific molecular tweezers are broad-spectrum inhibitors of assembly and toxicity of amyloid proteins, *J. Am. Chem. Soc. 133*, 16958-16969.

15. Attar, A., Chan, W. T., Klarner, F. G., Schrader, T., and Bitan, G. (2014) Safety and pharmacological characterization of the molecular tweezer CLR01 - a broad-spectrum inhibitor of amyloid proteins' toxicity, *BMC Pharmacol Toxicol 15*, 23.

16. Talbiersky, P., Bastkowski, F., Klärner, F. G., and Schrader, T. (2008) Molecular clip and tweezer introduce new mechanisms of enzyme inhibition, *J. Am. Chem. Soc. 130*, 9824-9828.

17. Prabhudesai, S., Sinha, S., Attar, A., Kotagiri, A., Fitzmaurice, A. G., Lakshmanan, R., Ivanova, M. I., Loo, J. A., Klarner, F. G., Schrader, T., Stahl, M., Bitan, G., and Bronstein, J. M. (2012) A novel "molecular tweezer" inhibitor of alpha-synuclein neurotoxicity in vitro and in vivo, *Neurotherapeutics 9*, 464-476.

18. Attar, A., Ripoli, C., Riccardi, E., Maiti, P., Li Puma, D. D., Liu, T., Hayes, J., Jones, M. R., Lichti-Kaiser, K., Yang, F., Gale, G. D., Tseng, C. H., Tan, M., Xie, C. W.,

Straudinger, J. L., Klärner, F. G., Schrader, T., Frautschy, S. A., Grassi, C., and Bitan, G. (2012) Protection of primary neurons and mouse brain from Alzheimer's pathology by molecular tweezers, *Brain 135*, 3735-3748.

19. Ferreira, N., Pereira-Henriques, A., Attar, A., Klärner, F. G., Schrader, T., Bitan, G., Gales, L., Saraiva, M. J., and Almeida, M. R. (2014) Molecular tweezers targeting transthyretin amyloidosis, *Neurotherapeutics 11*, 450-461.

20. Bohm, G., Muhr, R., and Jaenicke, R. (1992) Quantitative analysis of protein far UV circular dichroism spectra by neural networks, *Protein Eng 5*, 191-195.

21. Merabet, A., Houlleberghs, H., Maclagan, K., Akanho, E., Bui, T. T., Pagano, B., Drake, A. F., Fraternali, F., and Nikolova, P. V. (2010) Mutants of the tumour suppressor p53 L1 loop as second-site suppressors for restoring DNA binding to oncogenic p53 mutations: structural and biochemical insights, *The Biochemical journal 427*, 225-236.

22. Kayed, R., Head, E., Sarsoza, F., Saing, T., Cotman, C. W., Necula, M., Margol, L., Wu, J., Breydo, L., Thompson, J. L., Rasool, S., Gurlo, T., Butler, P., and Glabe, C. G. (2007) Fibril specific, conformation dependent antibodies recognize a generic epitope common to amyloid fibrils and fibrillar oligomers that is absent in prefibrillar oligomers, *Mol Neurodegener 2*, 18.

23. Joerger, A. C., and Fersht, A. R. (2007) Structural biology of the tumor suppressor p53 and cancer-associated mutants, *Adv Cancer Res 97*, 1-23.

24. Seifert, T., Bartholmes, P., and Jaenicke, R. (1984) Binding of the fluorescent dye 8-anilinonaphthalene 1-sulfonic acid to the native and pressure dissociated β 2-dimer of tryptophan synthase from Escherichia coli, *Zeitschrift fur Naturforschung. Section C: Biosciences 39*, 1008-1011.

25. Semisotnov, G. V., Rodionova, N. A., Razgulyaev, O. I., Uversky, V. N., Gripas, A. F., and Gilmanshin, R. I. (1991) Study of the "molten globule" intermediate state in protein folding by a hydrophobic fluorescent probe, *Biopolymers 31*, 119-128.

26. Shmueli, M. D., Schnaider, L., Rosenblum, D., Herzog, G., Gazit, E., and Segal, D. (2013) Structural Insights into the Folding Defects of Oncogenic pVHL Lead to Correction of Its Function In Vitro, *PloS one 8*, e66333.

27. Prabhudesai, S., Sinha, S., Attar, A., Kotagiri, A., Fitzmaurice, A. G., Lakshmanan, R., Ivanova, M. I., Loo, J. A., Klärner, F. G., Schrader, T., Stahl, M., Bitan, G., and Bronstein, J. M. (2012) A novel "molecular tweezer" inhibitor of α-synuclein neurotoxicity in vitro and in vivo, *Neurotherapeutics 9*, 464-476.

28. Rahimi, F., and Bitan, G. (2013) *Non-fibrillar Amyloidogenic Protein Assemblies—Common Cytotoxins Underlying Degenerative Diseases*, Springer.

29. Sinha, S., Du, Z., Maiti, P., Klärner, F. G., Schrader, T., Wang, C., and Bitan, G. (2012) Comparison of three amyloid assembly inhibitors: the sugar *scyllo*-inositol, the polyphenol epigallocatechin gallate, and the molecular tweezer CLR01, *ACS Chem. Neurosci. 3*, 451-458.

30. Silva, J. L., Gallo, C. V., Costa, D. C., and Rangel, L. P. (2014) Prion-like aggregation of mutant p53 in cancer, *Trends Biochem Sci*.

31. Silva, J. L., Rangel, L. P., Costa, D. C., Cordeiro, Y., and De Moura Gallo, C. V. (2013) Expanding the prion concept to cancer biology: dominant-negative effect of aggregates of mutant p53 tumour suppressor, *Biosci Rep 33*.

32. Rangel, L. P., Costa, D. C., Vieira, T. C., and Silva, J. L. (2014) The aggregation of mutant p53 produces prion-like properties in cancer, *Prion 8*.

33. Attar, A., and Bitan, G. (2014) Disrupting self-assembly and toxicity of amyloidogenic protein oligomers by " molecular tweezers" - from the test tube to animal models, *Curr. Pharm. Des. 20*, 2469-2483.

34. Bier, D., Rose, R., Bravo-Rodriguez, K., Bartel, M., Ramirez-Anguita, J. M., Dutt, S., Wilch, C., Klärner, F. G., Sanchez-Garcia, E., Schrader, T., and Ottmann, C. (2013) Molecular tweezers modulate 14-3-3 protein-protein interactions, *Nat. Chem. 5*, 234-239.

35. Wang, G., and Fersht, A. R. (2012) First-order rate-determining aggregation mechanism of p53 and its implications, *Proc Natl Acad Sci U S A 109*, 13590-13595.

36. Zheng, X., Liu, D., Klarner, F. G., Schrader, T., Bitan, G., and Bowers, M. T. (2015) Amyloid β-Protein Assembly: The Effect of Molecular Tweezers CLR01 and CLR03, *J. Phys. Chem. B 119*, 4831-4841.

37. Lopes, D. H., Attar, A., Nair, G., Hayden, E., Du, Z., McDaniel, K., Dutt, S., Bravo-Rodriguez, K., Mittal, S., Klarner, F. G., Wang, C., Sanchez-Garcia, E., Schrader, T., and Bitan, G. (2015) Molecular tweezers inhibit islet amyloid polypeptide assembly and toxicity by a new mechanism, *ACS Chem. Biol.*

38. Jarrett, J. T., and Lansbury, P. T., Jr. (1993) Seeding "one-dimensional crystallization" of amyloid: A pathogenic mechanism in Alzheimer's disease and scrapie?, *Cell 73*, 1055-1058.

39. Zheng, X., Liu, D., Klärner, F.-G., Schrader, T., Bitan, G., and Bowers, M. T. (2015) Amyloid β-protein Assembly: The Effect of Molecular Tweezer CLR01 and CLR03, *Submitted for publication*.

Funding Sources

This research was supported in part by grants from the Israel Science Foundation and the US Department of Defense (CDMRP) to DS and by the UCLA Jim Easton Consortium for Drug Discovery and Biomarker development to GB. GH acknowledges travel fellowships from Tel-Aviv University Center for Nanoscience and Nanotechnology.

Acknowledgments: We are indebted to Prof. Alan R. Fersht and Dr. Andreas C. Joerger, University of Cambridge, for generously hosting GH during part of this project and for their invaluable advice.

FIGURE LEGENDS

FIGURE 1. Illustration of the process of denaturation and subsequent aggregation of p53. Folded and unfolded p53 are in equilibrium, but unfolded p53 can irreversibly denature and form small, soluble aggregates, which cluster and precipitate over time. Adapted from (*3*).

FIGURE 2. Structure of the molecular tweezers. (**A**) CLR01; (**B**) CLR03. Reprinted with permission from Sinha *et al*., J. Am. Chem. Soc. 2011;133:16958-69. Copyright (2011) American Chemical Society.

FIGURE 3. Effect of molecular tweezers on thermo-stability of p53DBD. The effect of increased molar ratio of either CLR01 or CLR03 on stability of the G245S-p53DBD mutant was measured using differential scanning fluorimetry.

FIGURE 4. Effect of molecular tweezers on the early stage of p53DBD aggregation. The effect of CLR01 or CLR03 on the early stage of aggregation of G245S-p53DBD was monitored at 37 °C using ThT fluorescence (λ_{ex} = 450 nm, λ_{em} = 482 nm).

FIGURE 5. Effect of molecular tweezers on secondary structure of p53DBD. Far UV CD spectra of G245S-p53DBD in the absence or presence of increasing molar ratio of CLR01 or CLR03. CD spectra measurements were conducted at 37 °C after 20 min incubation. The table presents percentage of secondary structure calculated using the CDNN software (*20*).

FIGURE 6. p53DBD aggregation monitored by dot blot with antibody OC. Dot blot was performed using the OC antibody with pre-formed aggregates of G245S-p53DBD or R249S-p53DBD in the absence or presence of increasing molar ratio of CLR01 or CLR03.

FIGURE 7. Effect of molecular tweezers on the intermediate stage of p53DBD aggregation. The effect of increased molar ratio of CLR01 on the intermediate stage of aggregation of G245S-p53DBD was monitored at 37 °C, using static light scattering (λ = 500 nm).

FIGURE 8. Effect of molecular tweezers on the early stage of p53DBD folding/unfolding kinetics using ANS. The effect of 5-fold excess CLR01 or CLR03 on the early stage of conformational change kinetics of G245S-p53DBD or R249S-p53DBD was monitored at 37 °C using ANS fluorescence (λ_{ex} = 350 nm, λ_{em} = 400-560 nm). **(A)** ANS fluorescence spectra after 20 min incubation at 37°C. **(B)** λmax (465nm) plotted as a function of temperature.

FIGURE 9. Effect of molecular tweezers on the late stage of p53DBD aggregation. The effect of increased molar ratio of CLR01 on the late stage of aggregation of G245S-p53DBD **(A)** and R247S-p53DBD **(B)** was monitored at 37 °C, using turbidity (λ = 340 nm). (L) Indicates the lag phase; (F) the fast growth of aggregates and (P) the final stage of the aggregation reaction.

FIGURE 10. Effect of molecular tweezers on p53DBD morphology. Transmission electron micrographs of the aggregates of G245S-p53DBD **(A)** or R249S-p53DBD **(B)** at 37 °C in the absence or presence of increasing molar ratio of CLR01 or 1:10 molar ratio of CLR03, respectively. Scale bar: 1 μm. **(C)** Magnified view of areas with apparent fibrils of G245S-p53DBD:CLR01 in molar ratio of 1:2 or 1:5. Scale bar: 0.5 μm.

FIGURE 11. Effect of molecular tweezers on p53DBD-induced cytotoxicity. H1299 cells were grown for 24 hours. Cells were incubated for 24 hours with pre-formed aggregates of G245S-p53DBD or R249S-p53DBD in the absence or presence of increasing molar ratio of CLR01 or CLR03. Cell viability was measured using the

XTT assay. 0.1% Triton was used as a positive control. A. G245S-p53DBD Variant B. R249S-p53DBD Variant. Data are expressed as percent change compared to relevant control. P values were calculated by using the t.test; *p < 0.1, **p < 0.05, ***p < 0.001.

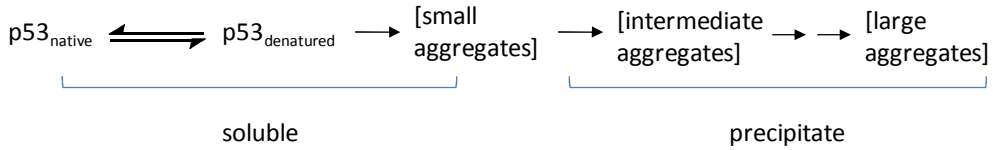

FIGURE 1.

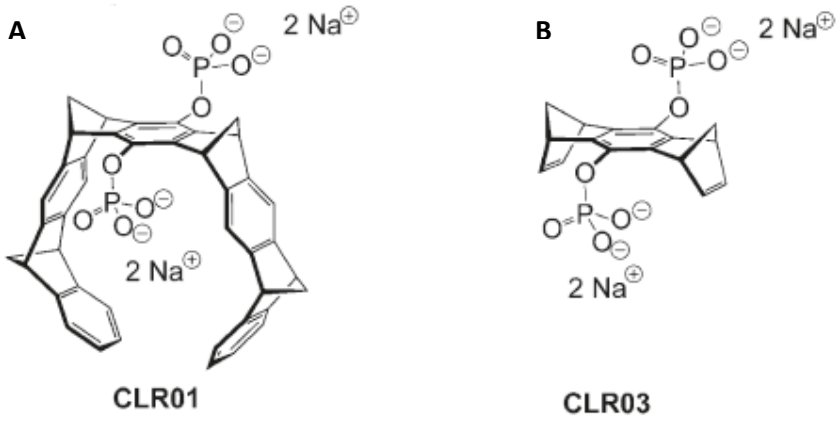

FIGURE 2.

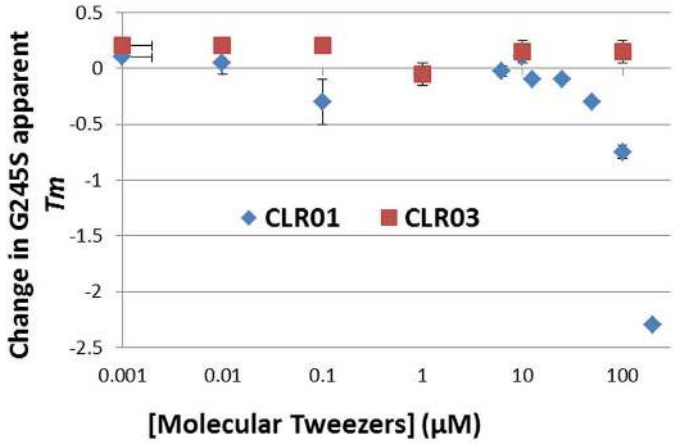

FIGURE 3.

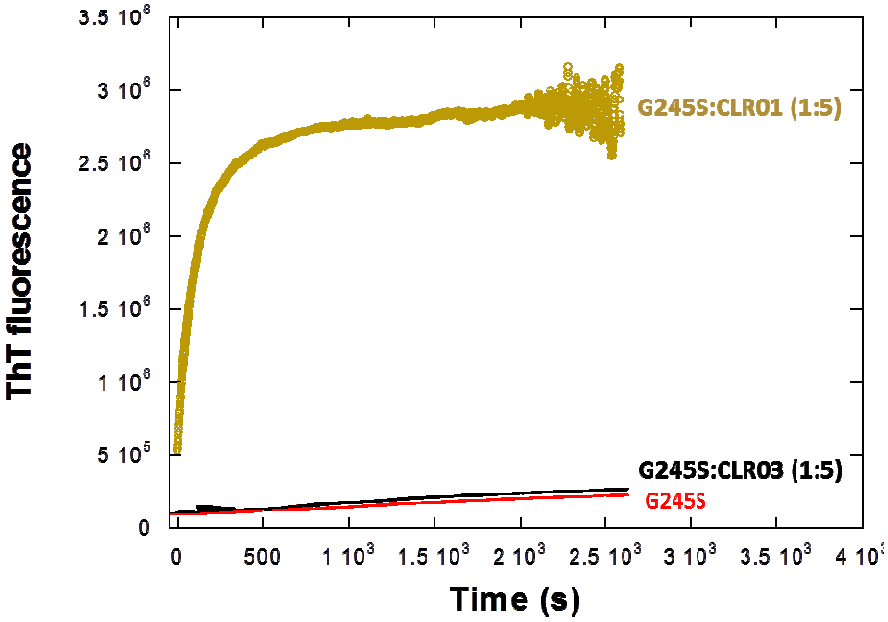

FIGURE 4.

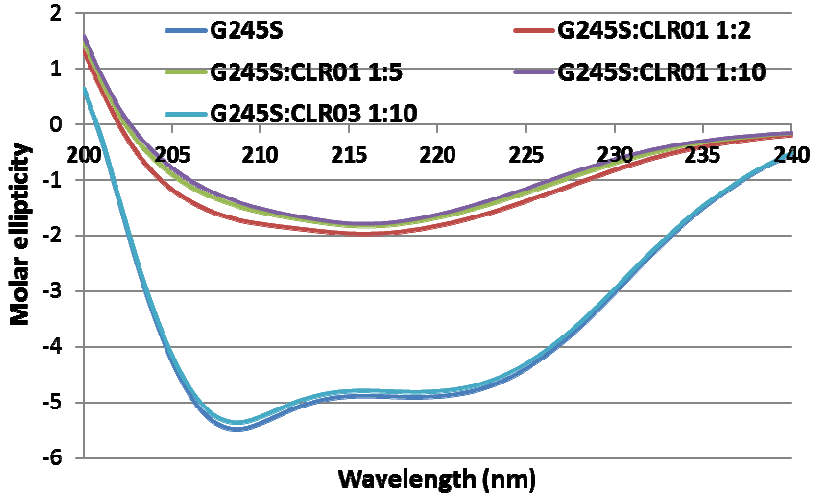

	Helix	Antiparallel	Parallel	Beta-Turn
G245S	63.5	2.7	3.1	12.9
G245S:CLR01 (1:2)	21.7	19.8	11.9	19.5
G245S:CLR01 (1:5)	18.4	23.8	12.8	17
G245S:CLR01 (1:10)	18.4	23.8	12.8	17
G245S:CLR03 (1:10)	42.4	6	6.6	15.6

FIGURE 5.

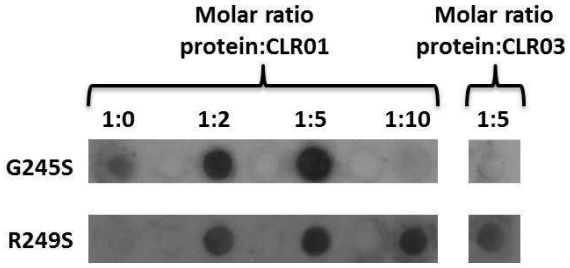

FIGURE 6.

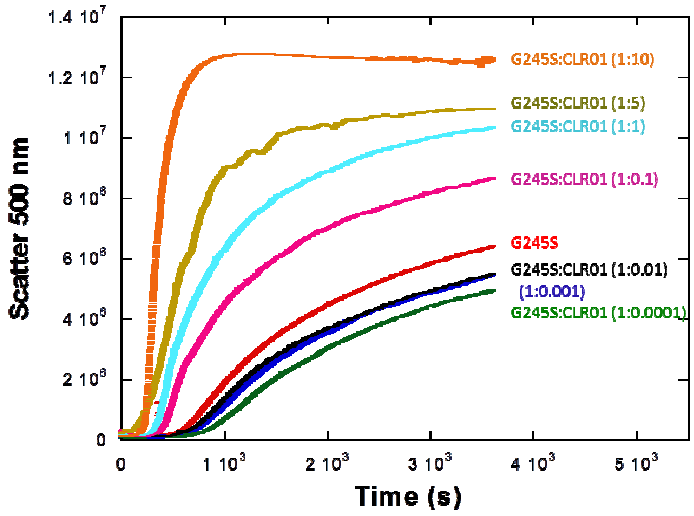
Scatter 500 nm
Time (s)
G245S:CLR01 (1:10)
G245S:CLR01 (1:5)
G245S:CLR01 (1:1)
G245S:CLR01 (1:0.1)
G245S
G245S:CLR01 (1:0.01)
(1:0.001)
G245S:CLR01 (1:0.0001)

FIGURE 7.

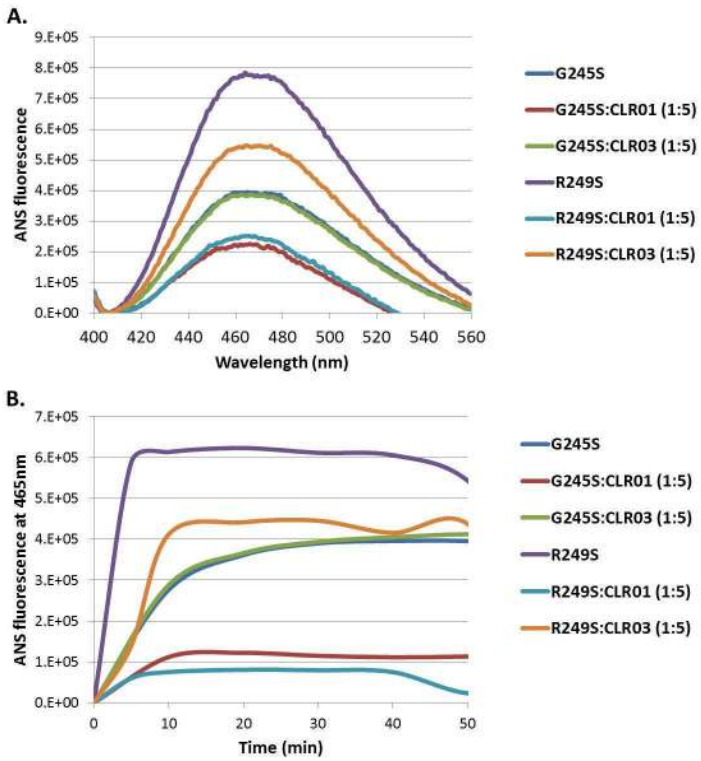
A.
ANS fluorescence
9.E+05
8.E+05
7.E+05
6.E+05
5.E+05
4.E+05
3.E+05
2.E+05
1.E+05
0.E+00
400 420 440 460 480 500 520 540 560
Wavelength (nm)
G245S
G245S:CLR01 (1:5)
G245S:CLR03 (1:5)
R249S
R249S:CLR01 (1:5)
R249S:CLR03 (1:5)
B.
ANS fluorescence at 465nm
7.E+05
6.E+05
5.E+05
4.E+05
3.E+05
2.E+05
1.E+05
0.E+00
0 10 20 30 40 50
Time (min)
G245S
G245S:CLR01 (1:5)
G245S:CLR03 (1:5)
R249S
R249S:CLR01 (1:5)
R249S:CLR03 (1:5)

FIGURE 8.

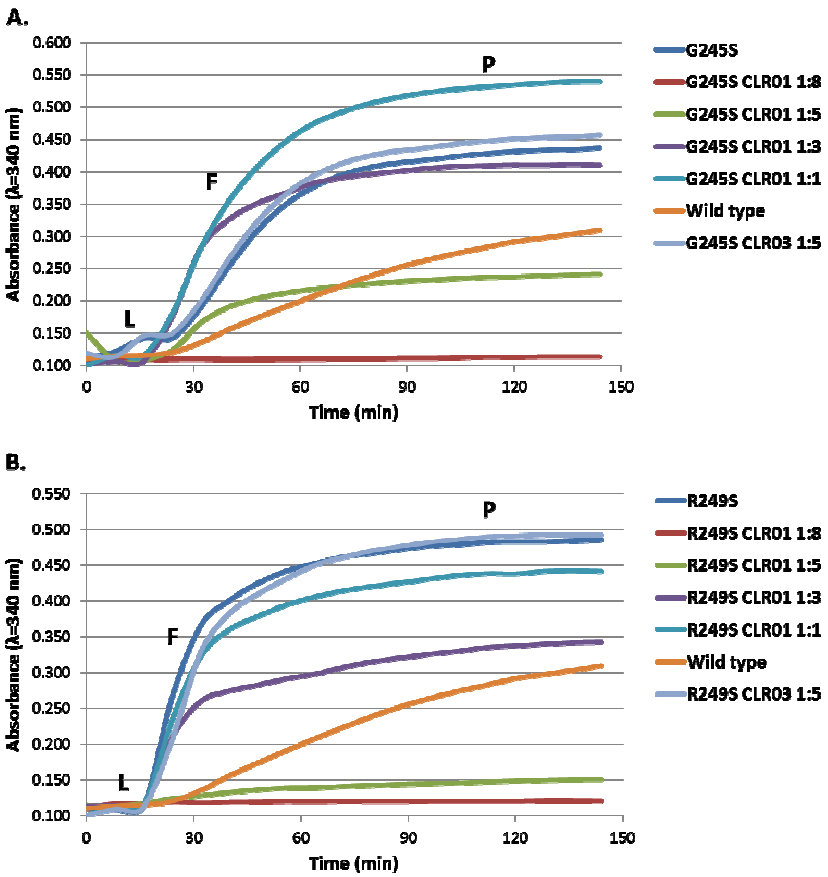
A.
Absorbance (λ=340 nm)
Time (min)
P
F
L
G245S
G245S CLR01 1:8
G245S CLR01 1:5
G245S CLR01 1:3
G245S CLR01 1:1
Wild type
G245S CLR03 1:5
B.
Absorbance (λ=340 nm)
Time (min)
P
F
L
R249S
R249S CLR01 1:8
R249S CLR01 1:5
R249S CLR01 1:3
R249S CLR01 1:1
Wild type
R249S CLR03 1:5

FIGURE 9.

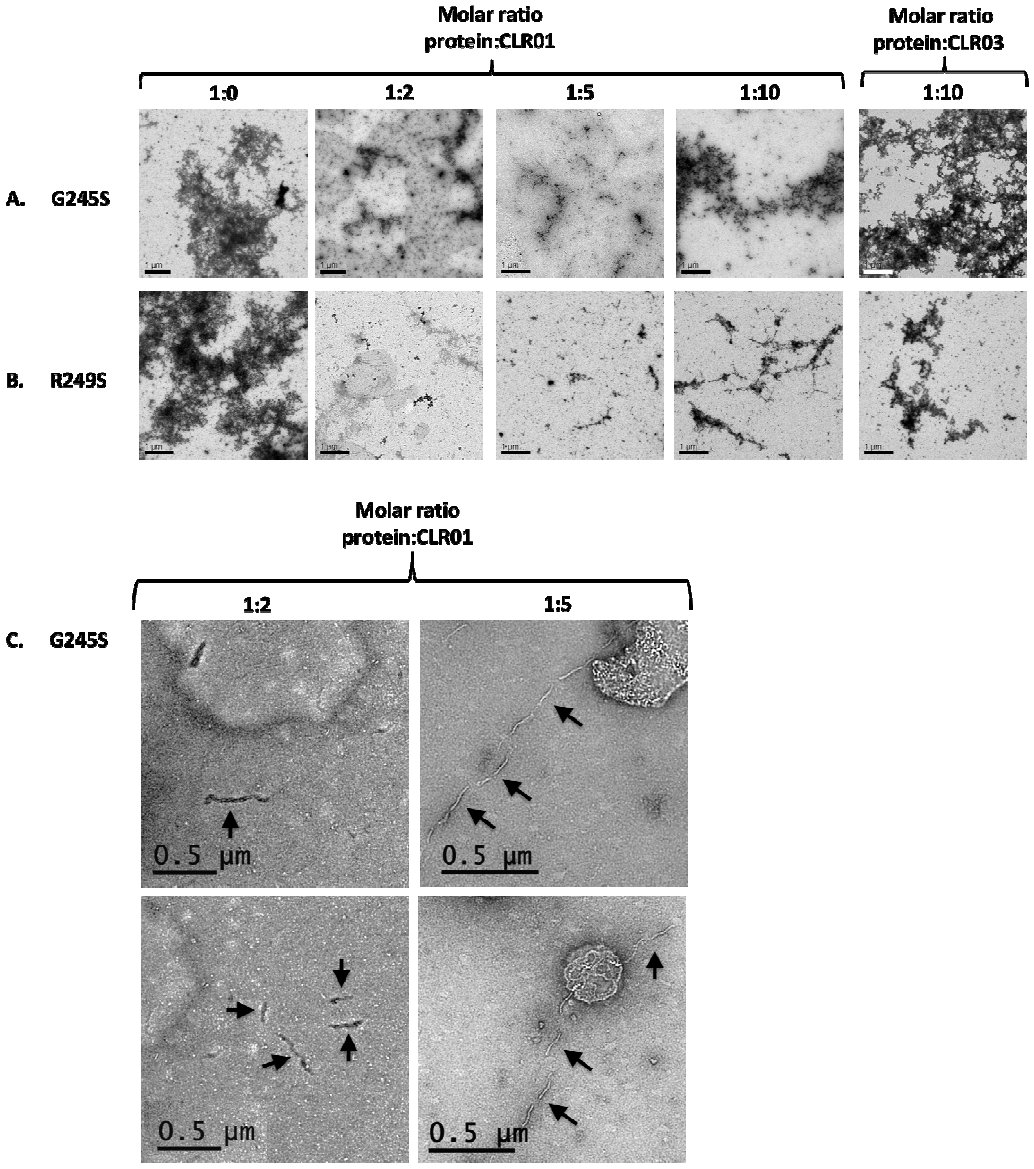
Molar ratio protein:CLR01
Molar ratio protein:CLR03
1:0
1:2
1:5
1:10
1:10
A. G245S
B. R249S
Molar ratio protein:CLR01
1:2
1:5
C. G245S
0.5 µm
0.5 µm
0.5 µm
0.5 µm

FIGURE 10.

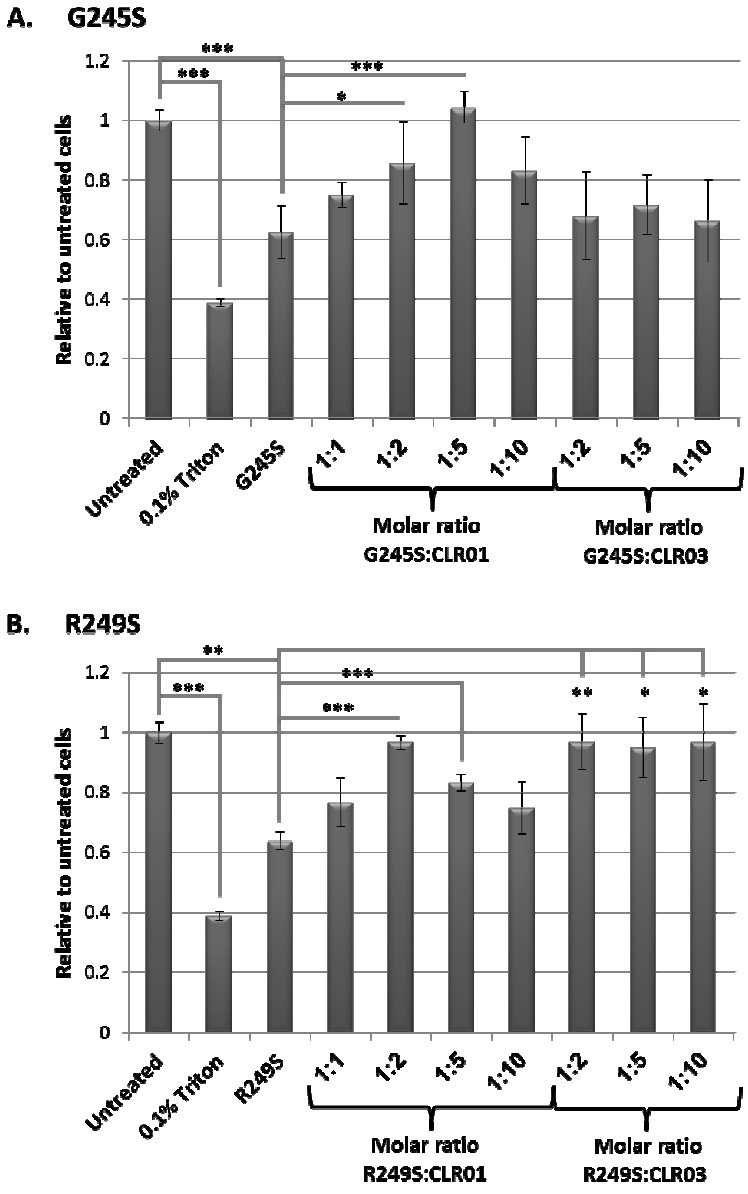
A. G245S
Relative to untreated cells
1.2
1
0.8
0.6
0.4
0.2
0
***
***
***
*
Untreated
0.1% Triton
G245S
1:1
1:2
1:5
1:10
1:2
1:5
1:10
Molar ratio G245S:CLR01
Molar ratio G245S:CLR03
B. R249S
Relative to untreated cells
1.2
1
0.8
0.6
0.4
0.2
0
**
***
***
**
*
*
Untreated
0.1% Triton
R249S
1:1
1:2
1:5
1:10
1:2
1:5
1:10
Molar ratio R249S:CLR01
Molar ratio R249S:CLR03

FIGURE 11.

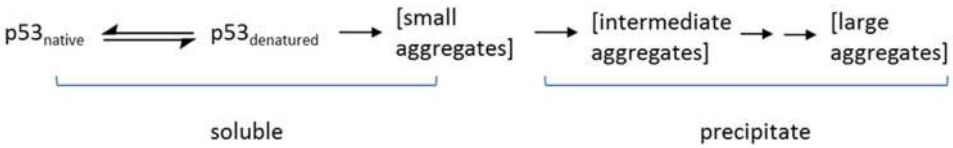

FIGURE 1. Illustration of the process of denaturation and subsequent aggregation of p53. Folded and unfolded p53 are in equilibrium, but unfolded p53 can irreversibly denature and form small, soluble aggregates, which cluster and precipitate over time. Adapted from (3).
82x13mm (300 x 300 DPI)

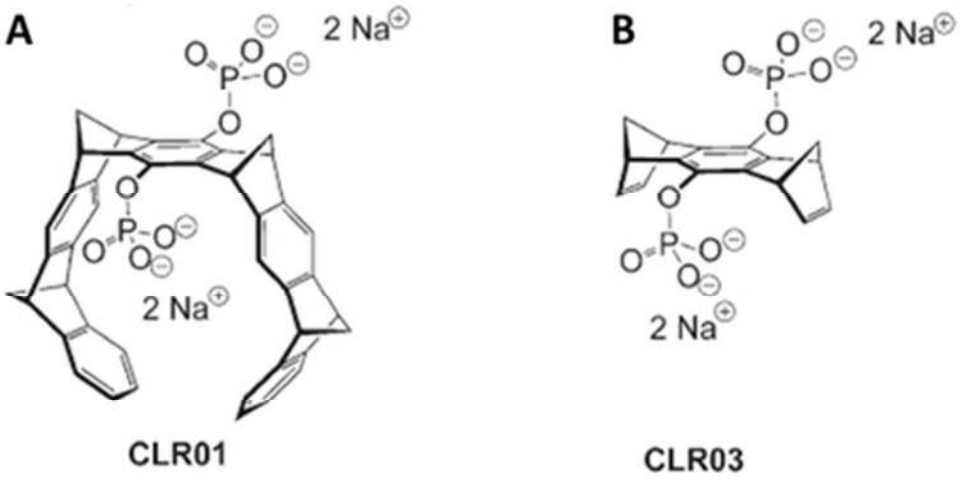

FIGURE 2. Structure of the molecular tweezers. (A) CLR01; (B) CLR03. Reprinted with permission from Sinha et al., J. Am. Chem. Soc. 2011;133:16958-69. Copyright (2011) American Chemical Society.
42x22mm (300 x 300 DPI)

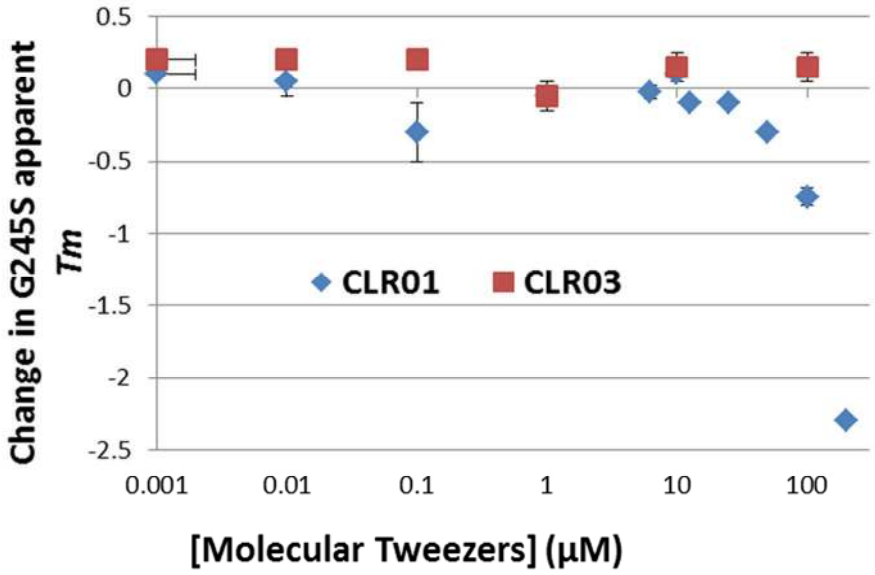

FIGURE 3. Effect of molecular tweezers on thermo-stability of p53DBD. The effect of increased molar ratio of either CLR01 or CLR03 on stability of the G245S-p53DBD mutant was measured using differential scanning fluorimetry.
82x49mm (300 x 300 DPI)

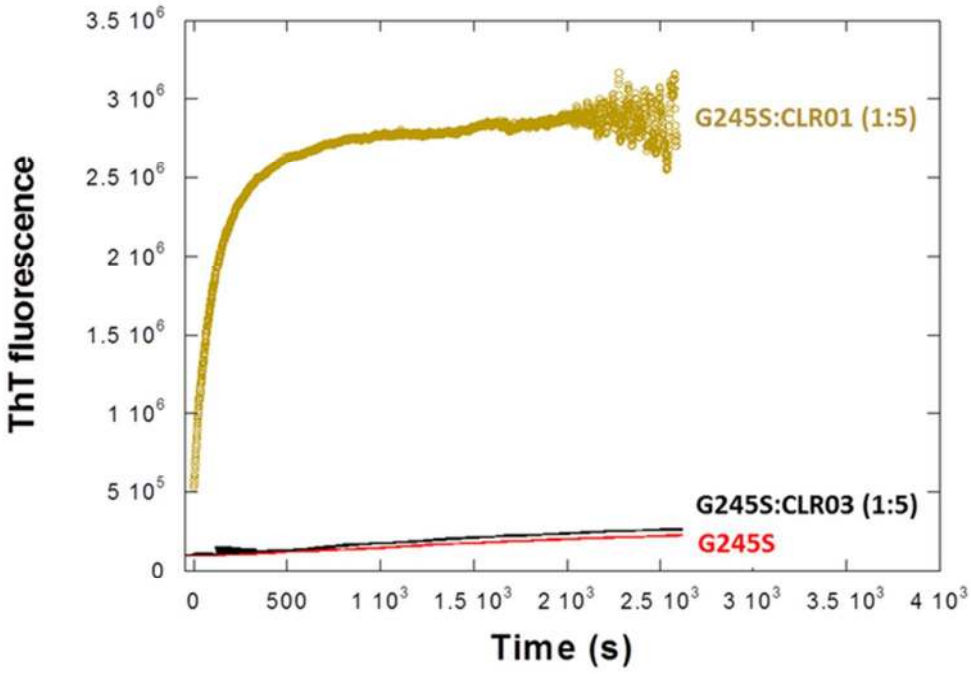

FIGURE 4. Effect of molecular tweezers on the early stage of p53DBD aggregation. The effect of CLR01 or CLR03 on the early stage of aggregation of G245S-p53DBD was monitored at 37 °C using ThT fluorescence (λex = 450 nm, λem = 482 nm).
58x42mm (300 x 300 DPI)

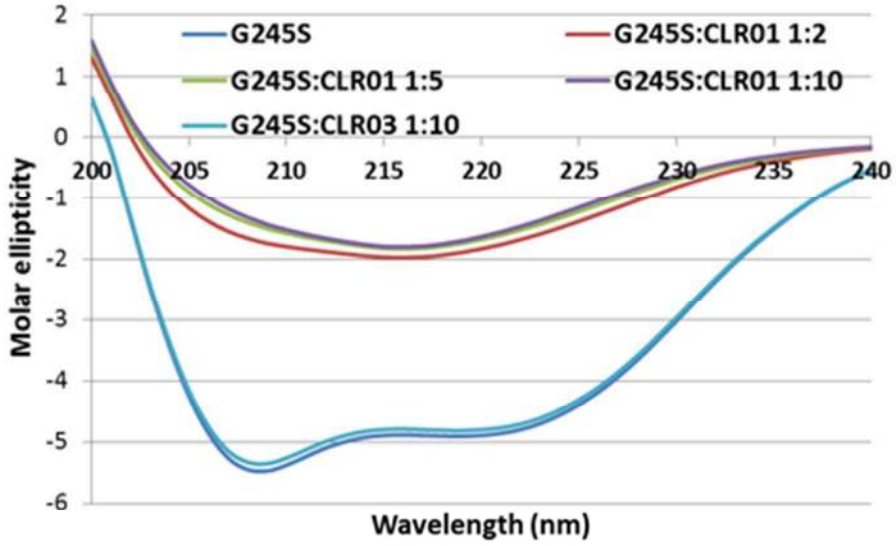

	Helix	Antiparallel	Parallel	Beta-Turn
G245S	63.5	2.7	3.1	12.9
G245S:CLR01 (1:2)	21.7	19.8	11.9	19.5
G245S:CLR01 (1:5)	18.4	23.8	12.8	17
G245S:CLR01 (1:10)	18.4	23.8	12.8	17
G245S:CLR03 (1:10)	42.4	6	6.6	15.6

FIGURE 5. Effect of molecular tweezers on secondary structure of p53DBD. Far UV CD spectra of G245S-p53DBD in the absence or presence of increasing molar ratio of CLR01 or CLR03. CD spectra measurements were conducted at 37 °C after 20 min incubation. The table presents percentage of secondary structure calculated using the CDNN software (36).
79x70mm (150 x 150 DPI)

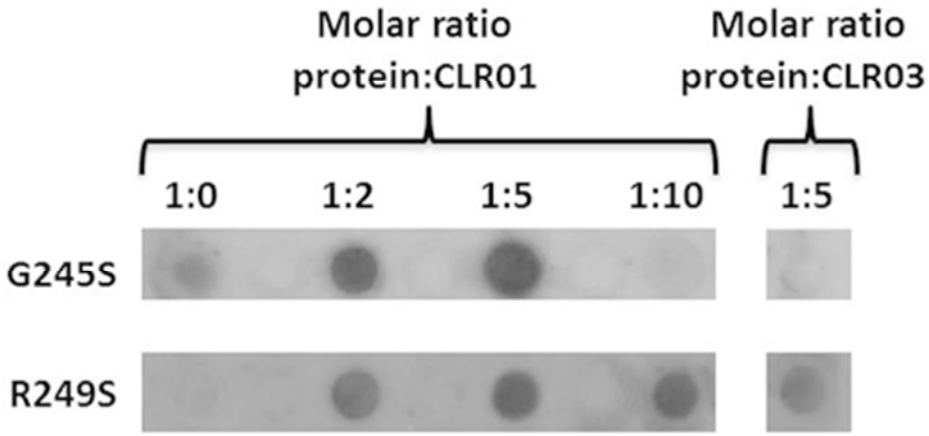

FIGURE 6. p53DBD aggregation monitored by dot blot with antibody OC. Dot blot was performed using the OC antibody with pre-formed aggregates of G245S-p53DBD or R249S-p53DBD in the absence or presence of increasing molar ratio of CLR01 or CLR03.
81x40mm (150 x 150 DPI)

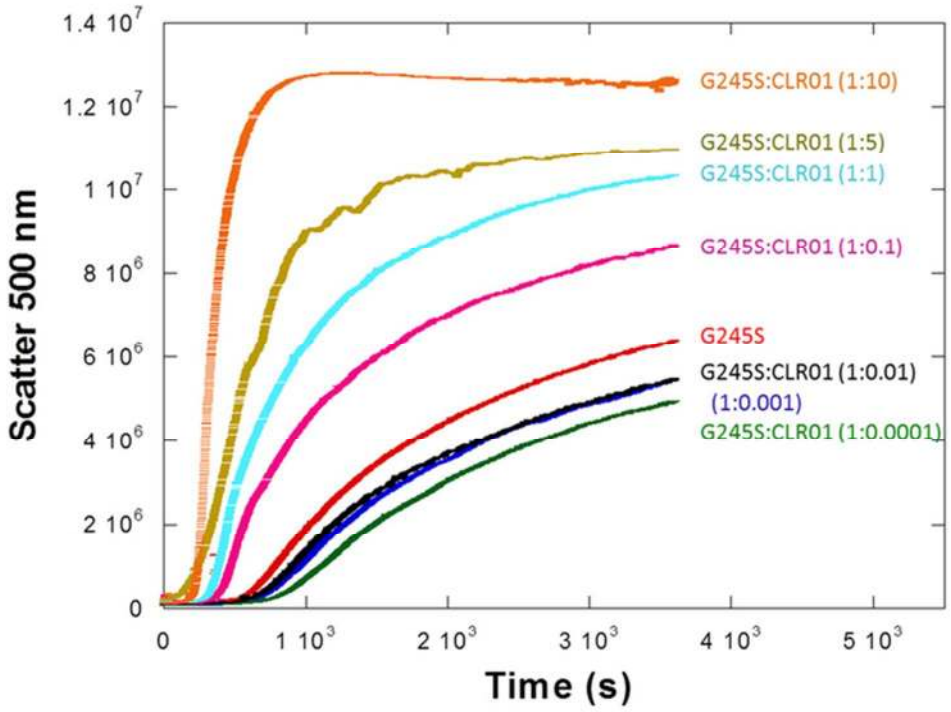

FIGURE 7. Effect of molecular tweezers on the intermediate stage of p53DBD aggregation. The effect of increased molar ratio of CLR01 on the intermediate stage of aggregation of G245S-p53DBD was monitored at 37 °C, using static light scattering (λ = 500 nm).
60x46mm (300 x 300 DPI)

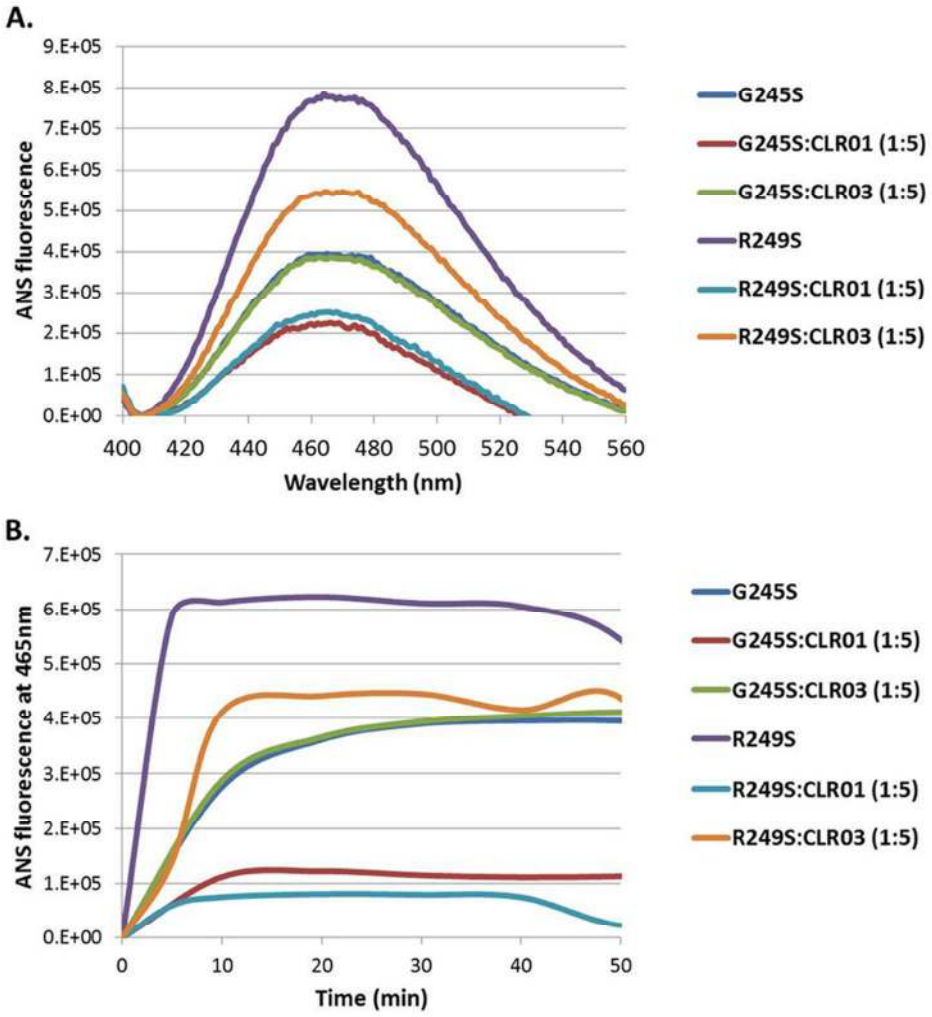

FIGURE 8. Effect of molecular tweezers on the early stage of p53DBD folding/unfolding kinetics using ANS. The effect of 5-fold excess CLR01 or CLR03 on the early stage of conformational change kinetics of G245S-p53DBD or R249S-p53DBD was monitored at 37 °C using ANS fluorescence (λex = 350 nm, λem = 400-560 nm). (A) ANS fluorescence spectra after 20 min incubation at 37°C. (B) λmax (465nm) plotted as a function of temperature.
86x90mm (300 x 300 DPI)

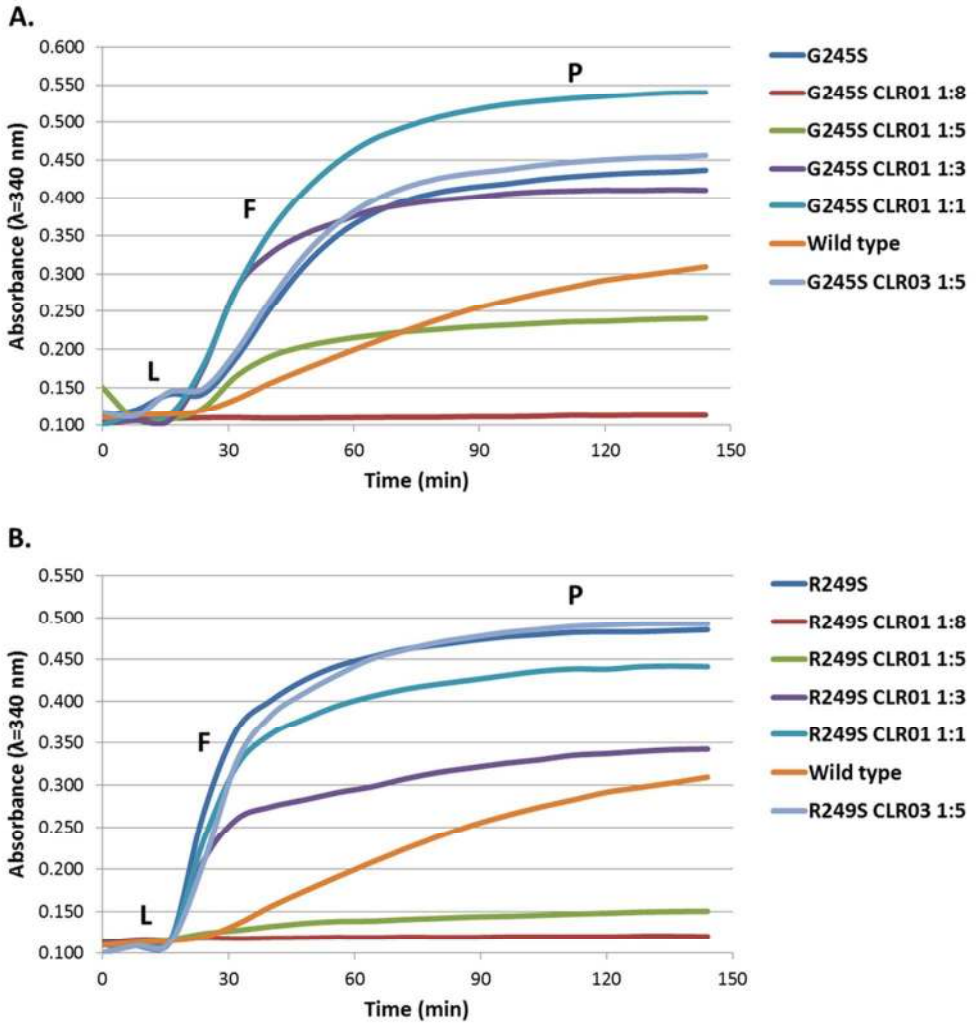

FIGURE 9. Effect of molecular tweezers on the late stage of p53DBD aggregation. The effect of increased molar ratio of CLR01 on the late stage of aggregation of G245S-p53DBD (A) and R247S-p53DBD (B) was monitored at 37 °C, using turbidity (λ = 340 nm). (L) indicates the lag phase; (F) the fast growth of aggregates and (P) the final stage of the aggregation reaction.
86x91mm (300 x 300 DPI)

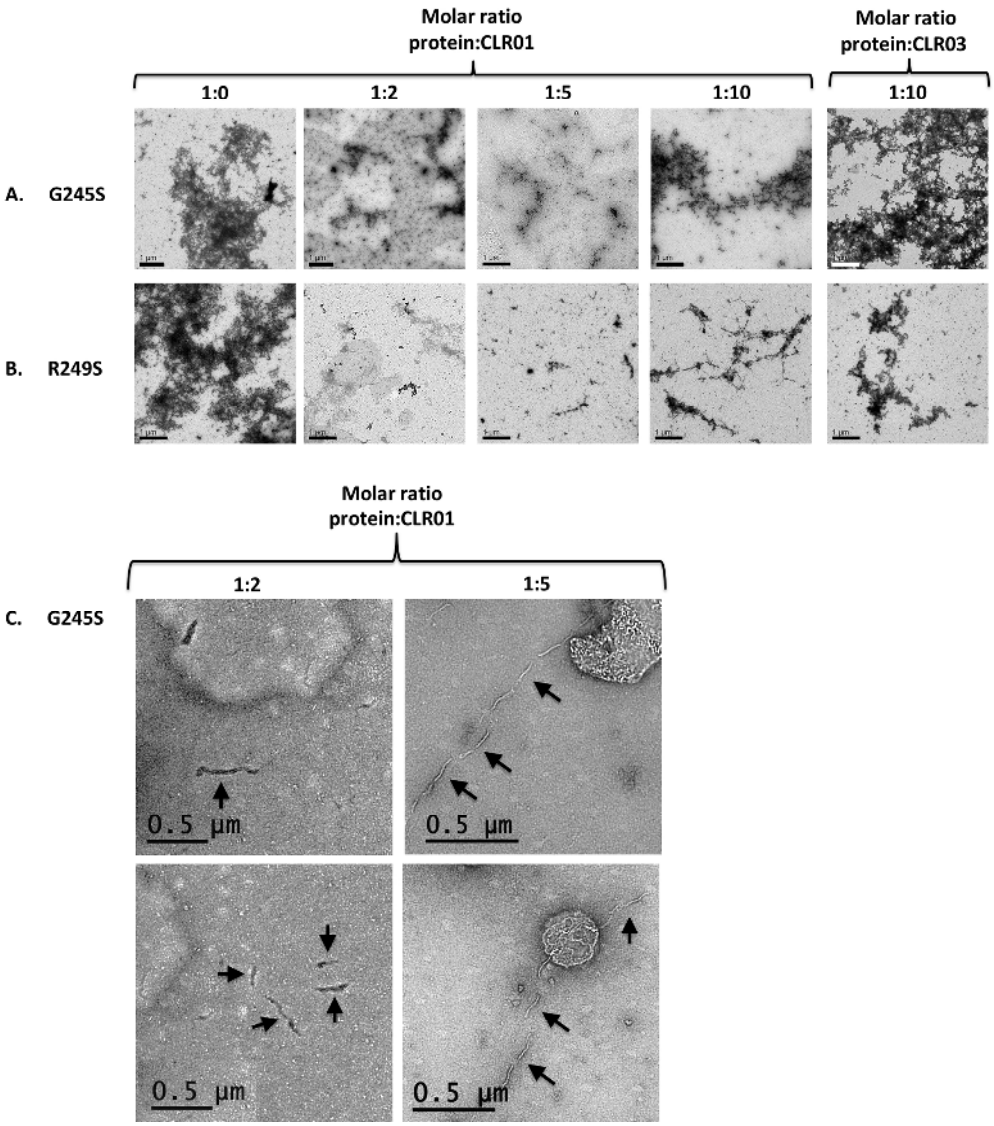

FIGURE 10. Effect of molecular tweezers on p53DBD morphology. Transmission electron micrographs of the aggregates of G245S-p53DBD (A) or R249S-p53DBD (B) at 37 °C in the absence or presence of increasing molar ratio of CLR01 or 1:10 molar ratio of CLR03, respectively. Scale bar: 1 µm. (C) Magnified view of areas with apparent fibrils of G245S-p53DBD:CLR01 in molar ratio of 1:2 or 1:5. Scale bar: 0.5 µm.
196x221mm (300 x 300 DPI)

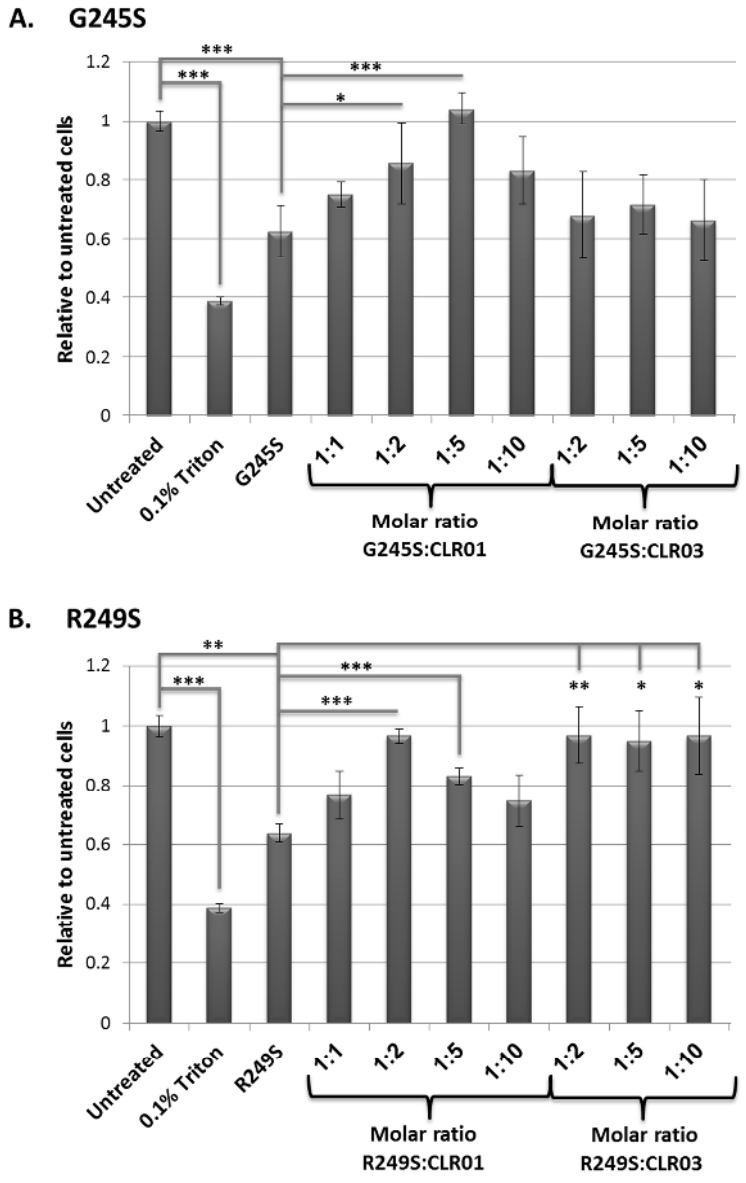

FIGURE 11. Effect of molecular tweezers on p53DBD-induced cytotoxicity. H1299 cells were grown for 24 hours. Cells were incubated for 24 hours with pre-formed aggregates of G245S-p53DBD or R249S-p53DBD in the absence or presence of increasing molar ratio of CLR01 or CLR03. Cell viability was measured using the XTT assay. 0.1% Triton was used as a positive control. A. G245S-p53DBD Variant B. R249S-p53DBD Variant. Data are expressed as percent change compared to relevant control. (**p < 0.05, ***p < 0.001).

124x195mm (300 x 300 DPI)

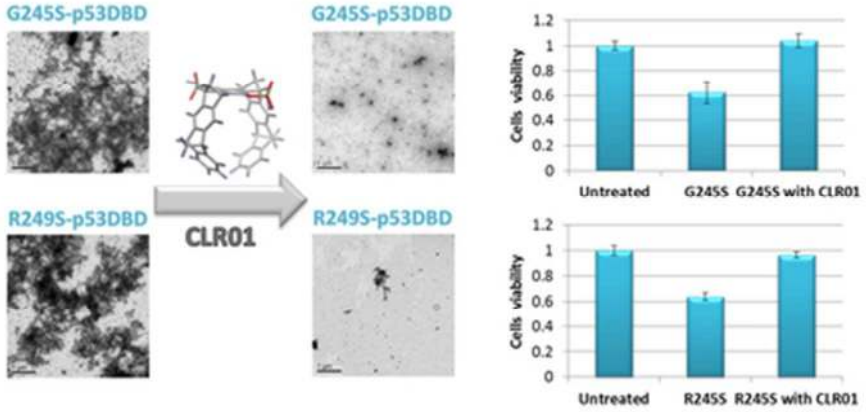

The effect of molecular tweezers on p53DBD
Transmission electron micrographs of the aggregates of G245S-p53DBD or R249S-p53DBD mutant proteins in the absence or presence of the molecular tweezer, CLR01. The molecular tweezer protects the cells from the harmful effect of the aggregates as observed by cell viability.

40x19mm (300 x 300 DPI)